Check for updates

Carbon quantum dots derived from the extracellular polymeric substance of anaerobic ammonium oxidation granular sludge for detection of trace Mn(VII) and Cr(VI)†

Fengli Liu,[a] Huosheng Li, [iD] *[b] Dandan Liao,[c] Yanhong Xu,[d] Mingxia Yu,[c] Shengwen Deng,[b] Gaosheng Zhang,[b] Tangfu Xiao,[c] Jianyou Long,[c] Hongguo Zhang,[c] Yuting Li,[a] Keke Li[c] and Ping Zhang*[a]

Carbon quantum dots (CQDs) were synthesized *via* a hydrothermal method, in which extracellular polymeric substance (EPS) from anaerobic ammonium oxidation (anammox) granular sludge was used as a carbon precursor, while citric acid and ethylenediamine were applied as auxiliary carbon source and passivation agent, respectively. The synthesized CQDs, with orderly spherical shape and mean size of 7.15 nm, emitted blue fluorescent light under UV radiation of 365 nm. The CQDs had a high fluorescence yield (40.84%), with good water solubility and excellent spectroscopic properties. In addition, the CQDs exhibited selective, sensitive and distinctive fluorescence quenching behaviors for Cr(VI) and Mn(VII) in a PBS buffer solution (NaH_2PO_4–Na_2HPO_4) of pH 7, with a detection limit of 5.8 nM for Cr(VI) and 2.3 nM for Mn(VII). Owing to the nitrogen components from the EPS of anammox granules, the CQDs were well nitrogen-doped, promoting electron-transfer and leading to reduction between the CQDs and Mn(VII)/Cr(VI). These results indicate that CQD-based chemical sensing is a simple and efficient means for the fluorescence detection of Mn(VII) and Cr(VI).

Introduction

The rapid development of modern industry has caused serious concerns over water contamination with respect to heavy metals.[1,2] Among the various heavy metals, chromium (Cr) is a toxic one with wide application in many industries, such as tannery, metallurgy, ceramics, cement, and pigment.[3] Hexavalent chromium (Cr(VI)) is nearly 100 times more toxic than trivalent chromium (Cr(III)),[4] therefore gaining significant attention for its detection and pollution control. Manganese (Mn) is another mostly used and concerning heavy metal, it is less toxic than Cr but exposure to excess Mn(VII) can also cause severe symptoms, such as irritability, neurological disorders and even genetic mutation.[5] Thus, it is necessary to develop simple, sensitive, and selective methods for the detection of these heavy metals.

Currently, the main assay methods for Mn(VII) and Cr(VI) are spectrophotometry with chromophoric reagents.[6] The spectrophotometric method usually requires specific pretreatment to improve the selectivity, and its sensitivity is often insufficient for detection at trace levels. Other detection methods, including flame atomic absorption spectrometry (FAAS), inductively coupled plasma-optical emission spectrometry (ICP-OES), and inductively coupled plasma-mass spectrometry (ICP-MS) are directly targeted at all of the valence states instead of the exact oxidation state of the metal.[7] Only when combining with special pretreatment methods can these expensive and sophisticated equipment be capable of determining the concentration of Mn(VII) and Cr(VI), which are in high oxidation valence.

Recently, the fluorescent probe techniques that utilize the carbon quantum dots (CQDs) or quantum dots (QDs) show a great potential as simple, fast, sensitive and selective means to determine the concentration of the heavy metals.[8] CQDs, defined as the carbon particles with size less than 10 nm, have been applied as fluorescence-based sensor of a variety of metal ions. Li *et al.* (2015) developed nitrogen and sulfur co-doped carbon dots to sensitively and selectively determine the concentration of Hg(II) ions.[9] Guo *et al.* (2018) successfully applied nitrogen and phosphor co-doped CQDs as chemosensor

[a]Key Laboratory for Water Quality and Conservation of the Pearl River Delta, Ministry of Education, College of Chemistry and Chemical Engineering, Guangzhou University, Guangzhou 510006, China. E-mail: zhangping@gzhu.edu.cn; Tel: +86 20 39366505

[b]Institute of Environmental Research at Greater Bay Area, Guangzhou University, Guangzhou 510006, China. E-mail: hilihuo@163.com

[c]School of Environmental Science and Engineering, Guangzhou University, Guangzhou 510006, China

[d]Key Laboratory of Three Gorges Reservoir Region's Eco-Environments of MOE, Chongqing University, Chongqing 400045, China

† Electronic supplementary information (ESI) available. See DOI: 10.1039/d0ra06133f

for detection of Fe(III) ions.[10] The CQDs or QDs have also recently been used for fluorescent-sensing of Mn(VII) and Cr(VI). Deng *et al.* (2017) established a method using phosphorescent L-cysteine modified manganese-doped zinc sulfide QDs to detect Mn(VII) anions,[7] with a detection limit of 0.24 μmol L^{-1}. Li *et al.* (2018) prepared a method using amino-functionalized CQDs for on-site chemosensing and quantitative determination of Cr(VI) in wastewater,[4] with a detection limit as low as 140 nmol L^{-1}. Despite of the previous success, the reported QDs-based methods for Mn(VII) and Cr(VI) detection still have some drawbacks, such as the complex functionalization/doping procedures and the relative low fluorescence yield and detection limit. There still is a need to develop a simpler QDs-based method with a lower limit for detection of Mn(VII) and Cr(VI). Some aspects including the source of the QDs, the preparation procedures, and the fluorescent sensing conditions could be further investigated.

To date, a variety of carbon sources have been tested for synthesis of CQDs. However, the extracellular polymeric substances (EPS) from a unique microorganism, anaerobic ammonium oxidation (anammox) bacteria, which are capable of converting ammonium and nitrite to dinitrogen gas under anoxic environment,[11] have not been reported to synthesize CQDs for heavy metal sensors.[12] Previous studies indicate that there are abundant polysaccharides, hydrophobic amino acids and proteins in the EPS of anammox granular sludge.[13,14] Conceivably, the EPS of anammox biomass may be a good source of the CQDs. Currently, there are no studies reported on applying anammox-based EPS to synthesize CQDs for quantification of heavy metal ions. The associated CQDs preparation method, and the chemosensing reaction conditions regarding the application of the CQDs derived from anammox-based EPS for determination of Mn(VII) and Cr(VI) still remain unclear.

Therefore, the purpose of this study is (1) to synthesize CQDs using the extract of EPS from anammox granular sludge, (2) to characterize the morphology, stability, spectroscopic property of the resultant CQDs, (3) to analyze the selectivity and sensitivity of the CQDs for detecting Mn(VII) and Cr(VI) anions.

Materials and methods

Materials

All reagents used were of analytical grade and directly used as received. Citric acid ($C_6H_8O_7$, CA), disodium hydrogen phosphate (Na_2HPO_4), potassium chloride (KCl) and quinine sulfate (($C_{20}H_{24}N_2O_2$)$_2 \cdot H_2SO_4 \cdot 2H_2O$) were purchased from McLean Biochemical Technology Co. Ltd. (Shanghai, China). Ethylenediamine ($C_2H_8N_2$) was purchased from Guangda Reagent Co. Ltd. (Guangdong, China). Dialysis bag (MWCO 3500, USA), sodium chloride (NaCl) were purchased from Best Chemical Co. Ltd. (Tianjin, China). Sodium dihydrogen phosphate (NaH_2PO_4) was purchased from Tianjin Yongda Chemical Reagent Co., Ltd. Metal salts ($NaNO_3$, $AgNO_3$, $CuSO_4$ $CaCl_2$, $Cr(NO_3)_3$, $MgSO_4$, $Ni(NO_3)_2$, $Pb(NO_3)_2$, $Sr(NO_3)_2$, $TlNO_3$, $KMnO_4$, $Zn(NO_3)_2$, $Cd(NO_3)_2$, $MnSO_4$, K_2CrO_4) were purchased from Aladdin Chemical Reagent Co. Ltd. (Shanghai, China). All water used was Milli-Q water with 18 MΩ cm resistance. The PBS buffer solution (0.1 mol L^{-1}) of pH 7 was prepared with 8.5 g NaCl, 2.2 g Na_2HPO_4 and 0.4 g Na_2HPO_4 in 100 mL Milli-Q water.

The extraction of EPS

The method for extraction of EPS from the anammox granular sludge was modified according to the study by Jia *et al.*[15] In brief, 200 mL of anammox granular sludge was collected and cleansed with deionized water. Next, the anammox biomasses were placed to a blender with addition of deionized water to obtain a suspension of 500 mL before they were being crushed for 5 min. After that, the resultant mixture was centrifuged at 5000*g* for 10 min and the bulk solution was collected as the EPS extract. The concentration of the total organic carbon of the EPS extract is shown in Table S1.†

Synthesis of CQDs

The synthesis of CQDs was modified according to the study by Li *et al.*[4] Firstly, 40 mL of the above-mentioned EPS extract solution and 1.34 mL of ethylene diamine were mixed with a stirrer, the resulted mixture was dosed with 4.204 g of citric acid. Secondly, the above mixture was transferred to a 50 mL polytetrafluoroethylene-lined stainless steel autoclave and heated at 200 °C for 5 h, then cooled to room temperature to obtain the raw CQDs solution. Thirdly, the resulted solution was placed in a dialysis bag (3.5 kDa molecular weight) and dialysed in the dark for 24 h to remove residual small molecular impurities. Finally, the CQDs powder was obtained after freeze-drying of the dialysed solution for 24 h. Notably, the dialysis membrane of 3.5 kDa molecular weight cut off was selected because the CQDs synthesized in this way had the highest fluorescent intensity when detected in the PBS buffer solution (pH = 7, NaH_2PO_4–Na_2HPO_4). In addition, the fluorescence quenching effect of the CQDs synthesized in this study was the strongest among the studied ones. The corresponding results are shown in (Fig. S1†).

Characterization

The total organic carbon was determined using a TOC analyzer (TOC-L CPH CN200, Kratos, Japan). A UV-Vis spectrophotometer (UV-6300, Shanghai, China) was used for spectrophotometric scanning and absorbance measurement (SUVA). A fluorescence spectrophotometer (F-4500, Hitachi, Japan) was used for wavelength scanning analysis. Fluorescence lifetime analysis was conducted using steady-state/transient fluorescence spectrometer (FLS920, Edinburgh, UK). A Fourier transform infrared (FT-IR) spectrometer (Tensor 27, Bruker Germany) was used to perform infrared spectroscopy for determination of functional groups. The crystalline structure was analyzed by X-ray diffraction (XRD) (PW3040/60, PANalytical Netherlands). Transmission electron microscopy (JEM-2010, JEOL, Japan) was used to analyze the morphological features. The specific surface area and pore size analyzer (SA3100, Beckman Kurt, American) were used to analyze the specific surface area and pore volume. A portable pH meter (PHB-3, Sanxin, Shanghai, China) was used to measure the pH value of the solution.

Fluorescent analysis

The as-prepared CQDs were dissolved in deionized water to obtain a solution of 0.1 mg mL^{-1} stock solution. Serial dilution of the stock solution was performed to attain a solution containing CQDs of 1 μg mL^{-1} for fluorescent analysis. The slit width was 5 nm, the scanning speed was 1200 nm min^{-1}, and the emission spectra were scanned in the range of 360–600 nm using 340 nm as the excitation wavelength.

For detection of metal ions, 3.0 mL of 1.0 μg mL^{-1} CQDs, 200 μL of different metal ion solutions, and 1.0 mL of PBS buffer solution (NaH$_2$PO$_4$–Na$_2$HPO$_4$) were added to the colorimetric tube in sequence, then deionized water was added to obtain a final volume of 10 mL, and the mixed liquid was immediately shaken. After 3 min, 3 mL of the above solution was sampled and measured with a cuvette at λ_{ex} = 360 nm and λ_{em} = 450 nm to record the fluorescence intensity. The concentration of the 15 metal ions, including Na$^+$, K$^+$, Mg^{2+}, Ni^{2+}, Pb^{2+}, Ca^{2+}, Sr^{2+}, Tl$^+$, Mn^{2+}, Cr^{3+}, Zn^{2+}, Cd^{2+}, MnO$_4^-$, CrO$_4^{2-}$, and Cu^{2+}, was 10 mmol L^{-1}. The fluorescence intensity with and without metal ion addition was denoted as F_0 and F, respectively, and the relative fluorescence intensity was F/F_0.

Quantum dot fluorescence attenuation spectrum

The fluorescence attenuation spectra of CQDs and Mn(VII) and Cr(VI) anions were determined by steady-state/transient fluorescence spectrometer.[16,17] The time-dependent single photon counting (TCSPS) principle is interpreted as follows. The sample emits a fluorescent photon signal upon the pulse light source excites the sample. For each pulse, only the time t of a single photon at a specific wavelength was recorded. After multiple counts, the probability distribution of the occurrence of fluorescent photons was measured. Among them, the average lifetime model was used to calculate the total lifetime of the time-resolved fluorescence spectrum (eqn (1)):

$$\tau = \sum \frac{A_n \tau_n^2}{A_n \tau_n} (n = 1, \ 2, \ 3...) \tag{1}$$

where A is the corresponding amplitudes; τ is the time constants of the radiative decay channels.

The fluorescence attenuation spectrum can be fitted with a double exponential function (eqn (2)):

$$I(t) = B_1 \exp\left(\frac{-t}{\tau_1}\right) + B_2 \exp\left(\frac{-t}{\tau_2}\right) \tag{2}$$

where B_1 and B_2 are two weights, τ_1 and τ_2 are two life factors, $I(t)$ is the fluorescence intensity decay at time t.

Calculation of fluorescence yield

Fluorescence quantum yield, which refers to the ratio of the number of photons emitted by the excited material to the number of photons absorbed by the excited material, is the most important index to measure the fluorescence performance of the CQD material. Quinine sulfate with a fluorescence quantum yield of 54% was used as the standard. The fluorescence quantum yield was determined by diluting sulfuric acid

quinine and carbon quantum dots, and measurement of related fluorescence intensity were calculated according to eqn (3).[18,19]

$$\Phi_{CQDs} = \Phi_{QS}(K_{CQDs}/K_{QS})(\eta_{CQDs}/\eta_{QS}) \tag{3}$$

Since η_{CQDs}/η_{QS} = 1, the formula for calculating the fluorescence yield of CQDs is reduced to eqn (4).

$$\Phi_{CQDs} = \Phi_{QS}(K_{CQDs}/K_{QS}) \tag{4}$$

where Φ is the relative quantum yield; K is the slope of the straight line; η is the solvent refractive index; subscripts CQDs and QS represent CQDs and quinine sulfate, respectively.

Results and discussion

Characterization of CQDs

The CQDs were fabricated *via* one-pot hydrothermal method (Fig. S2†), in which the anammox-EPS was used as the carbon precursors while ethylene diamine was applied as passivation agent. The TEM image shows the well-dispersed nanoparticles without apparent aggregation (Fig. 1a), exhibiting the typical dots-like appearance of CQDs, which are similar to previous studies.[20,21] In addition, the size distribution and average size of the synthesized CQDs are similar to those in literature.[21] The high-resolution TEM (HRTEM) image (Fig. 1b) of the CQDs reveals the lattice fringes with d-spacing of 0.21 nm and 0.12 nm, corresponding to the plane of (100) and (110) of graphite,[21,22] respectively. The orderly and clear lattice fringes indicate that the CQDs were successfully prepared. The particle size of obtained CQDs was in the range of 5.5–9.0 nm, with a mean diameter of 7.15 ± 0.83 nm (Fig. 1c), which is within the defined size of 10 nm for CQDs. The moderate graphitic structure of synthesized CQDs are in line with the previous study on nitrogen doped CQDs.[21] The XRD patterns (Fig. 1d) show a strong and broad diffraction peak at 2θ = 24.6°, and a weak diffraction peak at 2θ = 42.2° and another one at 2θ = 77.2°, which are assigned to the plane of (002), (100), and (110), respectively. The typical diffraction peak from (002) of CQDs is usually observed at 2θ = 26.4°,[21] however, the multiple components from the anammox-EPS may bond to the surface and expand the lattice spacing of the CQDs, and thus resulting in smaller diffraction angle compared to the previously reported value. According to the Bragg law (eqn (5)), the d-spacing of the lattice for (002) and (100) based on the diffraction peaks in Fig. 1d was determined to be 0.36 and 0.21 nm,[23] respectively, which are consistent with the results from Fig. 1b.

$$d = \frac{n\lambda}{2 \sin \theta} \tag{5}$$

where λ is the wavelength of incident X-rays (λ = 1.54 Å), and θ is the position of the related plane peak, n is a positive integer (1).

The calculation based on the N$_2$ gas sorption and desorption isotherms (Fig. 1e) shows that the BET specific surface area, the total pore volume and pore size of the CQDs were 59.03 m^2 g^{-1}, 0.3366 cm^3 g^{-1}, and 23.24 nm, respectively. The broad bands at 3391 cm^{-1}, 3257 cm^{-1}, and 2921 cm^{-1} were attributed to the stretching vibration of the –OH, N–H, and C–H groups,
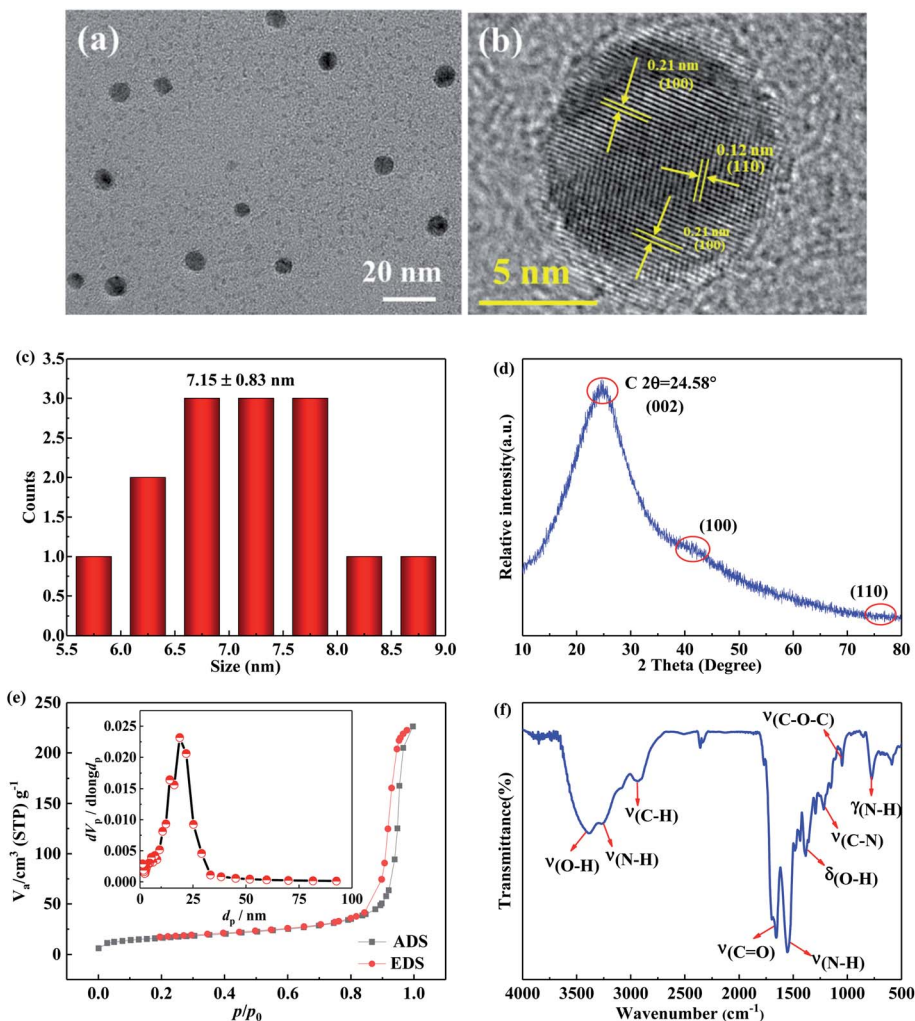
Fig. 1 Representative (a) TEM image, (b) HRTEM image showing lattice fringes and spacings, (c) particle size distribution histogram, (d) XRD patterns, (e) N₂ gas sorption and desorption isotherms, and (f) FT-IR spectra of the CQDs synthesized with anammox-EPS.

respectively.[24–26] The strong peaks at 1663 cm^{-1} was owing to the stretching vibration of the C=O bond, while the sharp peaks at 1553 cm^{-1} was owing to the bending vibration of the N–H bond,[4] indicating the nitrogen doped type of CQDs. The peak at 1388 cm^{-1} was due to the bending vibration of the –OH bond, while the peak at 1270 cm^{-1} was indicative of the C–N bond.[8,17] The band at 1020 cm^{-1} was assigned to the asymmetric and symmetric vibration of C–O–C bond, indicating the presence of –COOH groups. The peak at 770 cm^{-1} was owing to the out-of-plane bending vibration of N–H bond. The FT-IR spectra suggest that the –CO–NH– group originated from the amide bond was existed in the CQDs. The abundant surface groups on the CQDs enable their strong solubility in water, thus enhancing their stability and chemosensing ability.

The XPS spectra (Fig. 2a) show that three sharp and strong peaks at 284.9, 399.9, and 531.7 eV were observed, which are indicative of the XPS peaks of C 1s, N 1s, and O 1s, respectively. The major elemental composition was carbon (70.1%), followed by nitrogen (16.4%) and oxygen (12.9%). The fitting of the XPS of C 1s core level region (Fig. 2b) suggests the observation of four sub-peaks at 284.5 eV, 285.2 eV, 286.2 eV, and 287.9 eV,

corresponding to the C=C (sp^2)/C–C (sp^3), C–N, C–O, and C=O bonds, respectively.[21] The XPS of N 1s (Fig. 2c) indicates that there were two sub-peaks at 399.7 eV and 401.0 eV, which are assigned to the C–N–C and N–H bonds, respectively.[24] These results reveal the presence of the sp^2 C and amide bond. In addition, four sub-peaks were observed for the XPS of O 1s (Fig. 2d), in which the peaks at 530.1 eV, 531.1 eV, 532.1 eV, and 533.6 eV were assigned to the oxygen associated to the bonds of quinone, O=C–OH, C=O, and C–OH, respectively.[27] Therefore, the major elemental composition and the functionalized groups analyses (Fig. 2) imply that the synthesized materials were nitrogen doped CQDs with multiple surface bonds.

Spectral properties of the pure CQDs

The spectrophotometric and the fluorescent properties of the obtained CQDs were investigated (Fig. 3). As demonstrated in Fig. 3a, the two main absorption scopes were located in the ultraviolet region with wavelength of 200–250 nm and 300–400 nm, which were owing to the electron transition from π to π* taking place in the aromatic sp^2 carbon of CQDs.[22] The
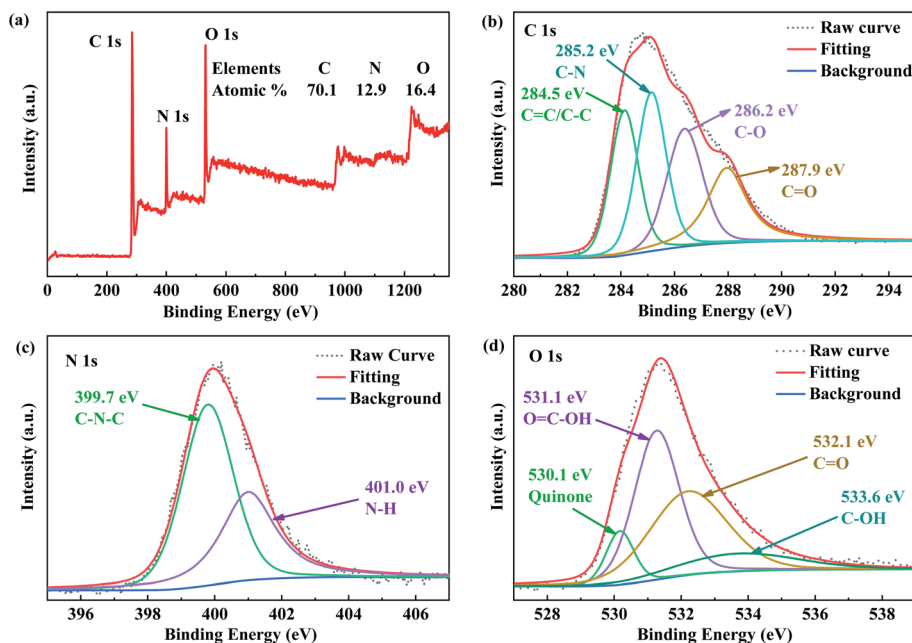
Fig. 2 XPS spectra: (a) survey, (b) C 1s core level, (c) N 1s core level, (d) O 1s core level of the CQDs synthesized with anammox-EPS.

maximum excitation and emission peaks were observed to be 340 nm and 450 nm, respectively. The characteristic absorption at 340 nm was consistent with maximum excitation fluorescence spectra. The original CQDs solution was in transparent yellow color, while it emitted bright blue fluorescence under radiation with a portable UV lamp of 365 nm. The fluorescence intensity spectra (Fig. 3b) show that the strongest fluorescence signal was located at 431 nm upon 340 nm excitation. Like most luminescent CQDs, the CQDs synthesized with anammox-EPS in this study also exhibited fluorescence behavior that depends on the excitation wavelength (λ_{ex}). As the λ_{ex} increased from 260 nm to 340 nm, the fluorescence intensity of emission peak gradually increased and reached the maximum at λ_{ex} = 340 nm. The further increase in λ_{ex} from 340 nm to 400 nm led to a stepwise decrease in the fluorescence intensity. Notably, the fluorescence spectra red-shifted slightly from 431 nm to 457 nm upon the increase in λ_{ex}. This excitation-dependent emission

phenomenon is also commonly observed in engineered CQDs, owing to the difference in surface defect states[28–30] or discrepancy in surface emissive trap sites.[31–33] The fluorescence spectra recorded at λ_{ex} of 360 nm and 320 nm, almost shared the same width and peak location as those of at λ_{ex} = 340 nm, indicating that the use of λ_{ex} in the range of 320–360 nm can achieve high and stable fluorescence intensity. The quantum yield of the CQDs with quinine sulfate as reference was calculated to be 40.8% (Fig. S3†), which is higher than that of many reported studies.[8,10,24,33] The high quantum yield may be beneficial to enhance the sensitivity of the detection of metal ions.

Spectral properties of the CQDs mixed with Mn(vii) or Cr(vi)

The influence of Mn(vii)/Cr(vi) on the optical property of CQDs was examined (Fig. S4† and 4). There were four UV/Vis absorption peaks observed at 310 nm, 348 nm, 526 nm, and 545 nm for the Mn(vii) solution (Fig. S4†), which are consistent
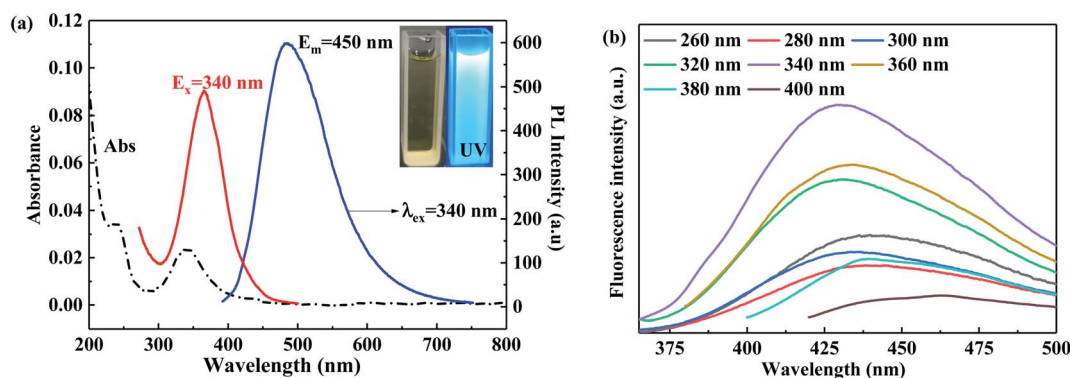

Fig. 3 (a) The UV/Vis absorbance, and the fluorescence emission spectra of the CQDs in water with λ_{ex} = 340 nm and λ_{em} = 450 nm. The inset photograph depicts the CQDs solution under visible light (left) and UV lamp (right) at 365 nm; (b) fluorescence intensity spectra of the CQDs at different λ_{ex} from 260 to 440 nm with an increment of 20 nm.
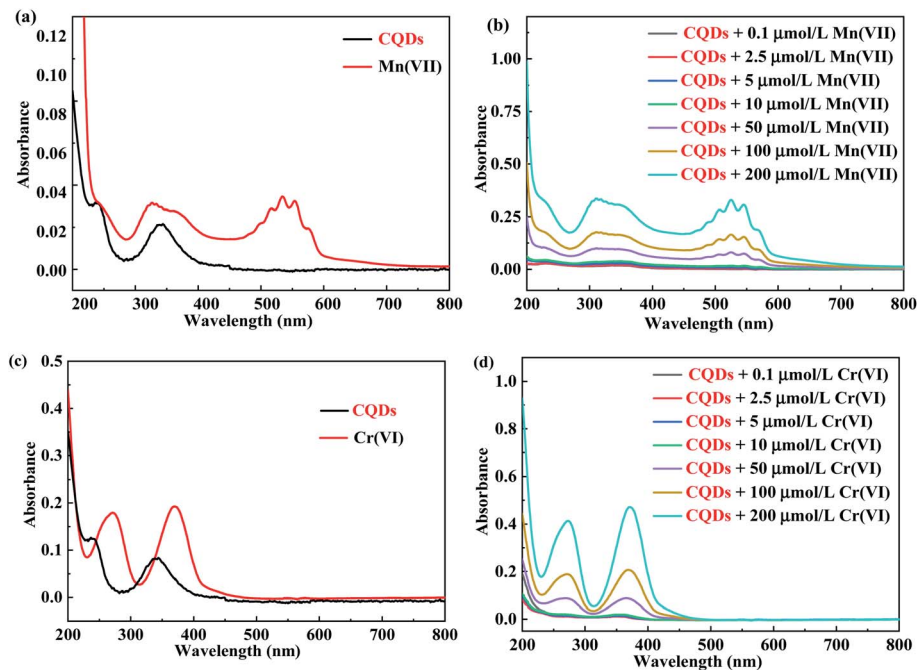
Fig. 4 (a) The UV/Vis absorbance of (a) respective solutions of CQDs (C_{CQDs} = 100 μmol L^{-1}) and Mn(VII) ($C_{Mn(VII)}$ = 100 μmol L^{-1}), (b) mixed solutions of CQDs and Mn(VII) at different concentrations, (c) respective solutions of CQDs and Cr(VI), and (d) mixed solutions of CQDs and Cr(VI) at different concentrations.

with the findings from previous study.[16] Interestingly, two peaks at λ_{ex} = 350 nm and λ_{em} = 450 nm for the CQDs overlapped with the UV/Vis absorption of Mn(VII), resulting in a possible inner filter effect (IFE) during the Mn(VII) assay.[28] Similarly, the Cr(VI) solution shared two absorption overlaps at 270 nm and 370 nm with the CQDs at λ_{ex} = 350 nm and λ_{em} = 450 nm. Therefore, both the Mn(VII) and Cr(VI) can be detected based on the IFE.

Compared with the Mn(VII) or the CQDs solution alone (Fig. 4a), the co-addition of both Mn(VII) and CQDs led to the disappearance of the absorbance feature of CQDs, only the spectral pattern of Mn(VII) was observed (Fig. 4b), owing to the IFE. The increase in the Mn(VII) concentration resulted in a stronger IFE and correspondingly larger UV/Vis absorbance, and thus a higher similarity to the Mn(VII) absorption spectra (Fig. 4b). Likewise, in comparison with the Cr(VI) or the CQDs solution alone (Fig. 4c), the mixing of both caused a completely overlap of the UV/Vis-based spectra of the Cr(VI) over that of the CQDs solution, only the spectra pattern of Cr(VI) solution was identified (Fig. 4d). The increase in Cr(VI) concentration from 0.1 μmol L^{-1} to 200 μmol L^{-1} resulted in a progressively higher UV/Vis absorbance, and thus closer similarity to the Cr(VI) absorption spectra (Fig. 4d). It should be noted that the increase in the concentration of Mn(VII) or Cr(VI) only led to the corresponding increase in the UV-Vis absorbance, there was no observed change in the shift of peaks. These phenomena enable the feasibility of using CQDs to quantify the concentration of Mn(VII) or Cr(VI) in aqueous solutions.

Stability of the CQDs

As shown from Fig. 5a, the increase in the concentration of KCl from 0 to 1.2 mol L^{-1} resulted in a progressive increase in the fluorescence intensity, while the further increased KCl addition caused a slight decrease followed by a slight increase in the fluorescence intensity. The addition of KCl was found to slightly enhance the fluorescence emission by 0–20% (Fig. 5b), indicating that the use of the CQDs to the assay of saline wastewater should take this strengthening effect into account. The fluorescence intensity of the CQDs increased with the increase in solution pH (Fig. 5b), then reached the peak value at the pH of 6–7 (Fig. 5c), and then decreased as solution pH continued to increase from 7 to 12. Therefore, the solution pH of 7 was chosen for the chemosensing pH value, which is similar to the previous study on Broccoli-based CQDs.[34] The photo-bleaching resistance of the CQDs was very strong (Fig. 5e), as ~90% of the original fluorescence intensity was observed even the CQDs solution was subjected to UV-radiation at room temperature for 2 h (Fig. 5f). Therefore, the CQDs obtained can be applied as a stable probe for detection of tracing metal ions under optimal conditions.

Selectivity of the CQDs

Compared to the various other metal ions, Mn(VII) and Cr(VI) ions were found to exhibit apparently lower photoluminescence when reacted with the CQDs (Fig. 6a). Fig. 6b shows that the Cr(VI) ions had a relative fluorescence intensity of 0.75, while the Mn(VII) ions had a lower one of 0.46. These observations enable the easy identification of the Mn(VII)/Cr(VI) from other cations. By harnessing this nature, the CQDs can be used as the probe to detect the concentration of Mn(VII)/Cr(VI) ions from water. Instant fluorescence quenching of the CQDs was observed by Mn(VII)/Cr(VI), since the fluorescence intensity immediately and dramatically decreased compared to that of the pure CQDs
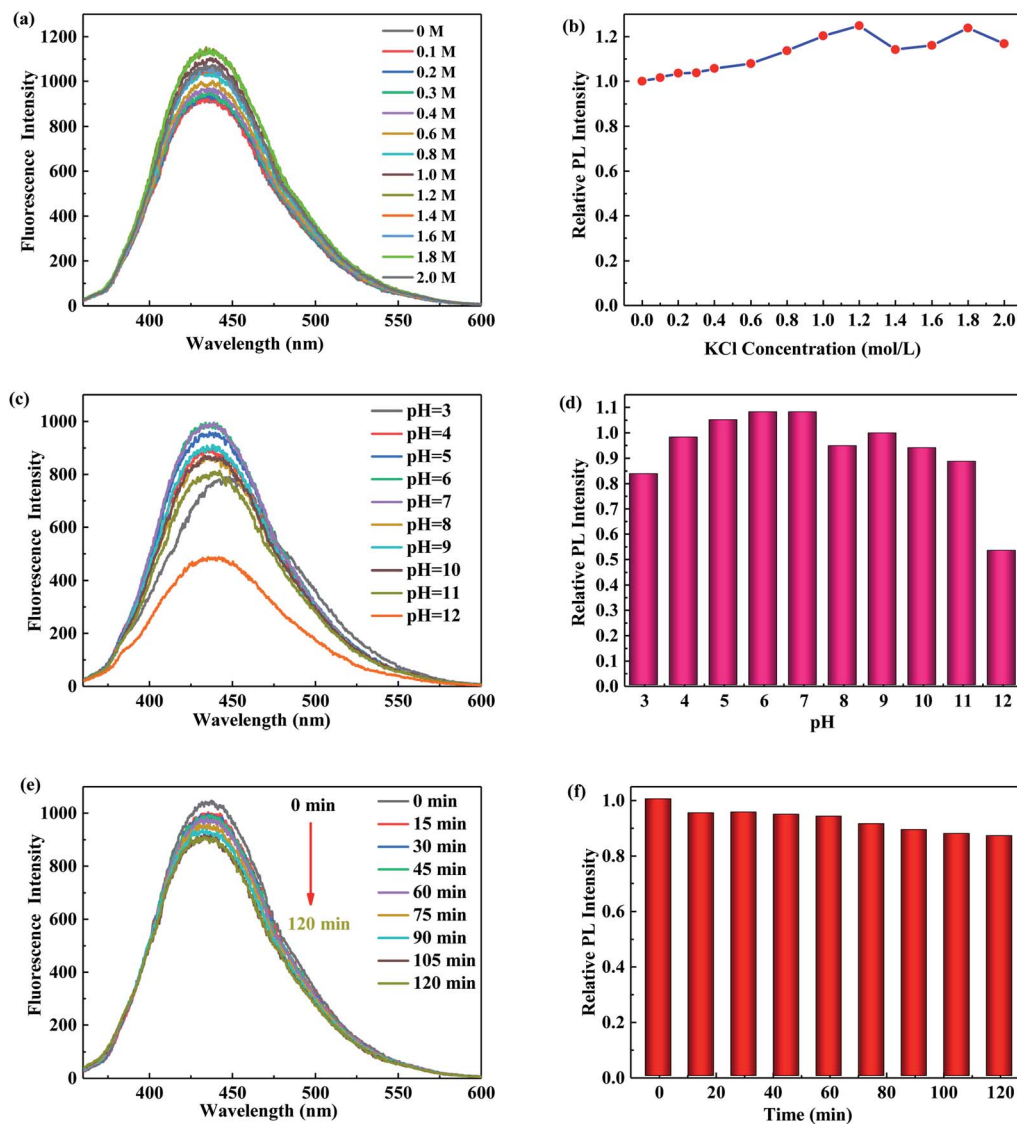
Fig. 5 Effect of different KCl concentration on (a) absolute and (b) relative fluorescence intensity; effect of different pH value on (c) absolute and (d) relative fluorescence intensity; effect of different radiation time on (e) absolute and (f) relative fluorescence intensity.

(Fig. 6c and d). The fluorescence responses were stable within 5 min, as there were no obvious changes in the fluorescence intensity. Considering the operability, the reaction time of 1 min was chosen as the optimum chemosensing time. In comparison to other studies,[6,34] the CQDs obtained in this study exhibited higher stability and selectivity as a probe to detect metal ions.

Quantum dot fluorescence attenuation spectra

To further investigate the mechanisms of fluorescence quenching of CQDs by Mn(VII)/Cr(VI), the fluorescence decay curves were recorded (Fig. 7). The three curves regarding the pure CQDs, the CQDs/Mn(VII), and CQDs/Cr(VI), were all well-fitted to the double-exponential function (eqn (2)) and all exhibited the same shape and similar patterns. The fitting and calculation (Table 1) indicate that the mean fluorescence

lifetime of the CQDs was 1.42 ns, which is shorter than that (6.37 ns) of N,S,P co-doped carbon nanodot in previous study,[35] likely because of the radiative recombination of carbon core excitations.[36] Notably, the fluorescence lifetime slightly increased to 2.22 ns for the CQDs/Mn(VII) and decreased to 0.74 ns for the CQDs/Cr(VI) system. These phenomena suggest that the fluorescence quenching of the CQDs by Mn(VII)/Cr(VI) involved a dynamic process with the IFE and other interactions.[37] The interaction between the CQDs and Mn(VII) could cause reduction of Mn(VIII) to Mn(II), and thus led to formation of Mn(II)-doped CQDs.[35] Thereupon, the improved exciton lifetime for Mn(II)-doped CQDs could be owing to the prolonged excitation localization between core excitons and carrier-surface-involved radiative recombination.[35] This radiation transition taking place between localized hole and electron quantized state could lead to a slower radiative recombination and thus subsequent higher photoluminescence emission
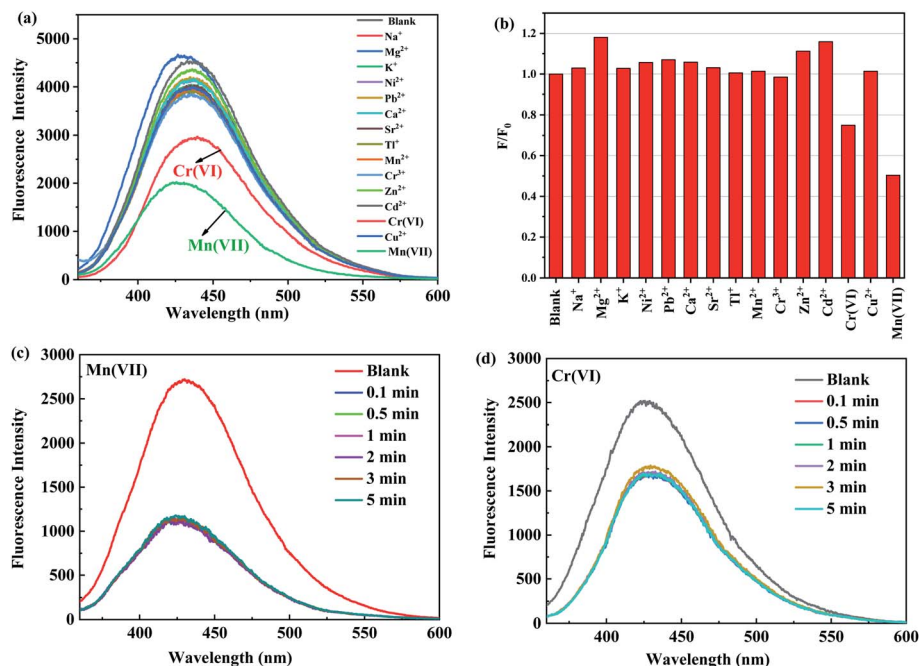
Fig. 6 (a) The fluorescence intensity of the CQDs reacted with different metal ions at a concentration of 10 mmol L^{-1}; (b) relative fluorescence intensity (F/F_0) of the CQDs interacted with different metal ions at a concentration of 20 mmol L^{-1}; fluorescence response of the CQDs with (c) Mn(VII) and (d) Cr(VI) concentration at radiation time from zero to 5 min.

Table 1 The obtained parameters of the dynamic fluorescence decay curves

Samples	B_1	$\tau_1/(ns)$	B_2	$\tau_2/(ns)$	$\tau/(ns)$
CQDs	1.57×10^3	20.0197	1.38×10^9	1.4221	1.4224
CQDs + Mn(VII)	1.16×10^7	2.18127	2047.641531	25.7244	2.2303
CQDs + Cr(VI)	1.76×10^7	0.73648	1.76×10^7	0.7365	0.7365

lifetimes.[35,38] The Cr(VI) could also react with the CQDs *via* reduction and *via* the surface sorption by the groups of –OH, –COOH and –NH$_2$, leading to the non-radiative recombination between the localized hole and electron transfer and thus the shorter photoluminescence emission lifetimes.[32,39]

Quantum yield

The fluorescence quenching percentage at different Mn(VII) concentrations (0–200 μmol L^{-1}) was linearly plotted against the absolute Mn(VII) concentrations to obtain the standard curves (Fig. S3†) and detection limit for the Mn(VII) (Fig. 8a and b). It is shown that (Fig. 8a) the photoluminescence of the mixed CQDs and Mn(VII) solution progressively decreased with the increase in concentration of Mn(VII) solution. The fluorescence quenching percentage ($(F_0 - F)/F_0$) was well linearly fitted with the absolute Mn(VII) concentrations (Fig. 8b). A linear standard curve ($Y = 0.00525X + 0.01916$) with R^2 value as high as 99.2% was achieved, and a relative standard deviation of the samples was as low as 0.010%. The detection limit of Mn(VII) was calculated to be 5.8 nmol L^{-1}, which is obtained by dividing the

3-fold standard deviation by the slope of the standard curve (Fig. 8b). This low detection limit suggests the high sensitivity of this material and method. In comparison to other studies,[6,28] the detection limit was much lower, revealing the great improvement in the sensitivity.

Similarly, the fluorescence intensity stepwise decreased with the increasing Cr(VI) concentration (Fig. 8c). The ratio of ($(F_0 - F)/F_0$) was also well fitted with the absolute Cr(VI) concentrations (Fig. 8d), with a linear relationship ($Y = 0.0135X + 0.1498$) of R^2 value as high as 98.0%. The relative standard deviation of the samples was as low as 0.010%. Therefore, the detection limit of Cr(VI) for this method was calculated to be 2.3 nmol L^{-1} using the above-mentioned method. This detection limit is much lower than that of many previous studies, for example, 140 nmol L^{-1},[4] 280 μmol L^{-1},[40] 400 nmol L^{-1},[41] 520 nmol L^{-1}.[42] The high

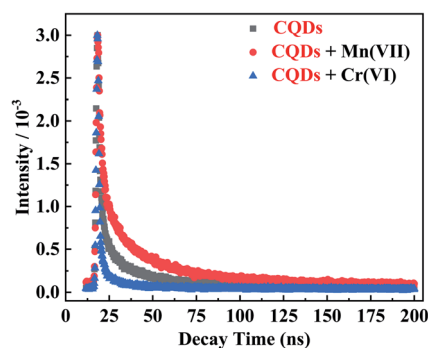**Fig. 7** The fluorescence decay curves for the CQDs and their mixed solution with Mn(VII)/Cr(VI).
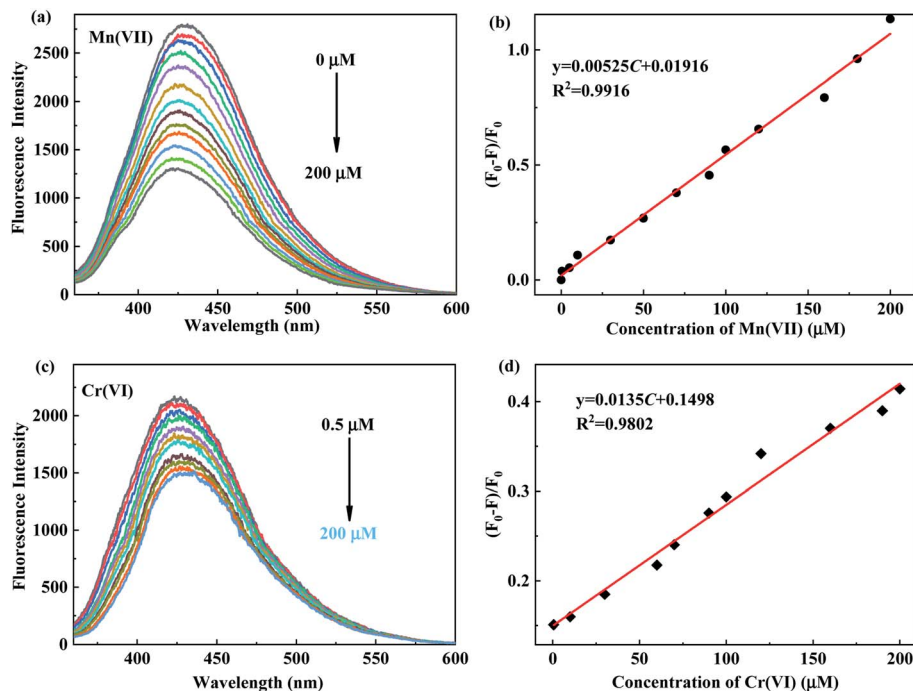
Fig. 8 (a) The fluorescence intensity of the CQDs reacted with different concentrations of Mn(VII); (b) the linear fitting of the ratio of $(F_0 - F)/F_0$ against Mn(VII) concentration; (c) the fluorescence intensity of the CQDs reacted with different concentrations of Cr(VI); (d) the linear fitting of the ratio of $(F_0 - F)$ to F_0 against Cr(VI) concentration (F: the end fluorescence intensity; F_0: the initial fluorescence intensity).

enhancement on the sensitivity suggests that this method can also be used as a probe to the quantitative determination of Cr(VI) concentration.

Conclusions

In summary, the extracellular polymer substance extracted from the granular sludge of the anaerobic ammonia oxidation bacteria can be successfully used as a carbon source to hydro-thermally synthesize CQDs for quantitative determination of Mn(VII) and Cr(VI) anions from water. The obtained CQDs have good fluorescence property, low toxicity, stability, water solubility, and high fluorescence quantum yield (40.8%). In addition, the CQDs have excellent selectivity for Mn(VII) and Cr(VI) in a PBS buffer solution system at pH = 7.0, and can be used as fluorescent probes to identify and quantitatively detect Mn(VII) and Cr(VI) anions, with detection limits of 5.8 nmol L^{-1} for Mn(VII) and 2.3 nmol L^{-1} for Cr(VI). This material and method in this study may have a promising application prospect in the field of fluorescent nanoprobes, environmental water quality monitoring, food sample monitoring and other biological applications.

Author contributions

Dr Huosheng Li and Prof. Ping Zhang conceived and designed the experiments; Miss Fengli Liu and Dr Huosheng Li wrote the paper; Miss Dandan Liao, Miss Yuting Li, Miss Mingxia Yu, Mr Shengwen Deng and Miss Keke Li performed the experiments, measurements and characterizations; Prof. Gaosheng Zhang,

Prof. Tangfu Xiao, Prof. Jianyou Long, Prof. Hongguo Zhang, and Dr Yanhong Xu analyzed the data and contributed to the analysis tools.

Conflicts of interest

There are no conflicts to declare.

Acknowledgements

References

1 H. Li, J. Xiong, G. Zhang, A. Liang, J. Long, T. Xiao, Y. Chen, P. Zhang, D. Liao, L. Lin and H. Zhang, *Sci. Total Environ.*, 2020, **698**, 134166.

2 Y. Li, H. Li, F. Liu, G. Zhang, Y. Xu, T. Xiao, J. Long, Z. Chen, D. Liao, J. Zhang, L. Lin and P. Zhang, *J. Hazard. Mater.*, 2020, **386**, 121900.

3 Q. Ge, X. Feng, R. Wang, R. Zheng, S. Luo, L. Duan, Y. Ji, J. Lin and H. Chen, *Environ. Sci. Technol.*, 2020, **54**, 8022–8031.

4 H.-Y. Li, D. Li, Y. Guo, Y. Yang, W. Wei and B. Xie, *Sens. Actuators, B*, 2018, **277**, 30–38.

5 Q. Hu, L. F. Liu, H. Sun, J. Han, X. Gong, L. Liu and Z. Q. Yang, *J. Food Compos. Anal.*, 2020, **88**, 103447.

6 X. Zhu, Y. Deng, P. Li, D. Yuan and J. Ma, *Microchem. J.*, 2019, **145**, 1135–1142.

7 P. Deng, L. Q. Lu, W. C. Cao and X. K. Tian, *Spectrochim. Acta, Part A*, 2017, **173**, 578–583.

8 M. Lu, Y. Duan, Y. Song, J. Tan and L. Zhou, *J. Mol. Liq.*, 2018, **269**, 766–774.

9 L. Li, B. Yu and T. You, *Biosens. Bioelectron.*, 2015, **74**, 263–269.

10 Y. Guo, F. Cao and Y. Li, *Sens. Actuators, B*, 2018, **255**, 1105–1111.

11 H. S. Li, S. Q. Zhou, Y. J. Qin, J. Y. Long, F. S. Zheng and H. G. Zhang, *Desalin. Water Treat.*, 2019, **149**, 1–10.

12 M. Boleij, H. Kleikamp, M. Pabst, T. R. Neu, M. C. M. van Loosdrecht and Y. Lin, *Environ. Sci. Technol.*, 2020, **54**, 5218–5226.

13 M. Boleij, M. Pabst, T. R. Neu, M. C. M. van Loosdrecht and Y. M. Lin, *Environ. Sci. Technol.*, 2018, **52**, 13127–13135.

14 C. Feng, T. Lotti, Y. Lin and F. Malpei, *Chem. Eng. J.*, 2019, **374**, 112–122.

15 F. Jia, Q. Yang, X. Liu, X. Li, B. Li, L. Zhang and Y. Peng, *Environ. Sci. Technol.*, 2017, **51**, 3260–3268.

16 X. Gong, Z. Li, Q. Hu, R. Zhou, S. Shuang and C. Dong, *ACS Appl. Mater. Interfaces*, 2017, **9**, 38761–38772.

17 Z. Feng, Z. Li, X. Zhang, G. Xu and N. Zhou, *J. Mater. Sci.*, 2018, **53**, 6459–6470.

18 W. Gao, H. Song, X. Wang, X. Liu, X. Pang, Y. Zhou, B. Gao and X. Peng, *ACS Appl. Mater. Interfaces*, 2017, **10**, 1147–1154.

19 L. S. Li, X. Y. Jiao, Y. Zhang, C. Cheng, K. Huang and L. Xu, *Sens. Actuators, B*, 2018, **263**, 426–435.

20 K. Hola, M. Sudolska, S. Kalytchuk, D. Nachtigallova, A. L. Rogach, M. Otyepka and R. Zboril, *ACS Nano*, 2017, **11**, 12402–12410.

21 R. Atchudan, T. Edison and Y. R. Lee, *J. Colloid Interface Sci.*, 2016, **482**, 8–18.

22 S. Huang, E. Yang, J. Yao, Y. Liu and Q. Xiao, *Anal. Chim. Acta*, 2018, **1035**, 192–202.

23 R. Atchudan, S. Perumal, T. N. Jebakumar Immanuel Edison and Y. R. Lee, *Mater. Lett.*, 2016, **166**, 145–149.

24 D. Gu, S. Shang, Q. Yu and J. Shen, *Appl. Surf. Sci.*, 2016, **390**, 38–42.

25 J. Chen, J. Zhang, J. Liu, Y. He, F. Evrendilek, M. Buyukada, W. Xie and S. Sun, *Chem. Eng. J.*, 2020, **397**, 125372.

26 J. Zhang, G. Sun, J. Liu, F. Evrendilek and M. Buyukada, *J. Cleaner Prod.*, 2020, **253**, 119950.

27 Y. J. Oh, J. J. Yoo, Y. I. Kim, J. K. Yoon, H. N. Yoon, J.-H. Kim and S. B. Park, *Electrochim. Acta*, 2014, **116**, 118–128.

28 F. Du, G. Li, X. Gong, G. Zhonghui, S. Shuang, M. Xian and C. Dong, *Sens. Actuators, B*, 2018, **277**, 492–501.

29 Y. Guo and W. Zhao, *Spectrochim. Acta, Part A*, 2020, **240**, 118580.

30 L. S. Li, X. Y. Jiao, Y. Zhang, C. Cheng, K. Huang and L. Xu, *Sens. Actuators, B*, 2018, **263**, 426–435.

31 Y. Dong, H. Pang, H. B. Yang, C. Guo, J. Shao, Y. Chi, C. M. Li and T. Yu, *Angew. Chem., Int. Ed. Engl.*, 2013, **52**, 7800–7804.

32 J. H. He, Y. Y. Cheng, T. Yang, H. Y. Zou and C. Z. Huang, *Anal. Chim. Acta*, 2018, **1035**, 203–210.

33 M. Shamsipur, K. Molaei, F. Molaabasi, M. Alipour, N. Alizadeh, S. Hosseinkhani and M. Hosseini, *Talanta*, 2018, **183**, 122–130.

34 N. Arumugam and J. Kim, *Mater. Lett.*, 2018, **219**, 37–40.

35 S. A. Rub Pakkath, S. S. Chetty, P. Selvarasu, A. Vadivel Murugan, Y. Kumar, L. Periyasamy, M. Santhakumar, S. R. Sadras and K. Santhakumar, *ACS Biomater. Sci. Eng.*, 2018, **4**, 2582–2596.

36 L. Wang and H. S. Zhou, *Anal. Chem.*, 2014, **86**, 8902–8905.

37 S. Song, F. Liang, M. Li, F. Du, W. Dong, X. Gong, S. Shuang and C. Dong, *Spectrochim. Acta, Part A*, 2019, **215**, 58–68.

38 S. S. Chetty, S. Praneetha, S. Basu, C. Sachidanandan and A. V. Murugan, *Sci. Rep.*, 2016, **6**, 26078.

39 H. Liu, Z. He, L. P. Jiang and J. J. Zhu, *ACS Appl. Mater. Interfaces*, 2015, **7**, 4913–4920.

40 T. Tian, Y. He, Y. Ge and G. Song, *Sens. Actuators, B*, 2017, **240**, 1265–1271.

41 Y. Ma, Y. Chen, J. Liu, Y. Han, S. Ma and X. Chen, *Talanta*, 2018, **185**, 249–257.

42 J. Shen, S. Shang, X. Chen, D. Wang and Y. Cai, *Sens. Actuators, B*, 2017, **248**, 92–100.